https://doi.org/10.5194/egusphere-2023-1927
Preprint. Discussion started: 9 October 2023

Retrieval of sea ice drift in the Fram Strait based on data from Chinese satellite HaiYang (HY1-D)

Dunwang Lu[1,2,3], Jianqiang Liu[2,3](deceased), Lijian Shi[2,3], Tao Zeng[2,3], Bin Cheng[4], Suhui Wu[2,3], ManmanWang[1,2,3]

[1] National Marine Environmental Forecasting Center, Beijing 100081, China
[2] National Satellite Ocean Application Service, Beijing 100081, China
[3] Key Laboratory of Space Ocean Remote Sensing and Application, Ministry of Natural Resources, Beijing 100081, China
[4] Finnish Meteorological Institute, Helsinki 00101, Finland

Correspondence to: Lijian Shi (shilj@mail.nsoas.org.cn)

Abstract. Melting of sea ice in the Arctic ocean has accelerated due to global warming. The Fram Strait (FS) serves as a crucial pathway for sea ice export from the Arctic to the North Atlantic Ocean. Monitoring sea ice drift (SID) in FS provides insights into how Arctic sea ice responds to the climate change. The SID has been retrieving from Sentinel-1 SAR, AVHRR, MODIS and AMSR-E, and using optical data to retrieve SID still needs further exploration. In this paper, we retrieve SID in the FS using China's HaiYang1-D (HY1-D) satellite equipped with the Coastal Zone Imager (CZI). Multi-template matching technique is employed to calculate cross-correlation, and subpixel estimation is used to locate displacement vectors from the cross-correlation matrix. The dataset covering March to May 2021 is divided into hourly and daily intervals for analysis, and validation is performed using Copernicus Marine Environment Monitoring Service (CMEMS) SAR-based product and IABP buoy measurements. Comparison with CMEMS SID product reveals a high correlation at the daily level; however, due to spatial and temporal variability in sea ice motion, differences are observed at an hourly resolution. Additionally, validation against IABP buoy data shows a velocity bias of 0.004 m/s and RMSE of 0.027 m/s at the day-level, along with a flow direction bias of 0.057 rad and RMSE of 0.313 rad respectively; while at the hour-level, velocity bias is negligible (0 m/s), with an RMSE value of 0.022 m/s; similarly for flow direction bias which remains negligible. During the validation against buoys, we find that the accuracy of retrieving the SID flow direction is highly interrelated with the sea ice displacement.

1 Introduction

The Arctic, as one of the three poles of the Earth (Li et al., 2020) that stores 101,000 km^3 of fresh water (Finnish Meteorological Institute et al., 2022), is an important part of the cryosphere and plays an important role in global water and atmospheric cycles. Since the beginning of the twenty-first century, global warming has profoundly affected human production and activities and has become an important factor threatening the stability of the climate system (Cook et al., 2014). Under the effect of Arctic amplification (Serreze et al., 2009), Arctic quick warming accelerates the melting of polar sea ice, leading to accelerated sea ice break-up and sea ice transport (Krumpen et al., 2016; Maslanik et al., 2011). The acceleration of sea ice motion also

https://doi.org/10.5194/egusphere-2023-1927
Preprint. Discussion started: 9 October 2023

indicates a decrease in the residence time of sea ice in the Arctic (Sumata et al., 2023). Moreover, the changes in sea ice feed back into the climate system, affecting energy transport (Dethloff et al., 2006; Döscher et al., 2014).

Sea ice drift (SID) is an important geophysical parameter that describes the movements of sea ice, and it is the process of sea ice as it moves across the sea surface in response to winds, currents and other forces (gravity, Coriolis effect, etc.) (Encyclopedia of Ocean Sciences, 2022). The large-scale SID over the Arctic consists of the Beaufort Gyre (BG) and the Transpolar Drift (TPD) (Preller and Posey, 1989), and the TPD transports large quantities of multiyear ice outward from the central Arctic toward the FS (Colony and Thorndike, 1984; Martin and Augstein, 2000). The FS connects the Arctic and the North Atlantic (Sumata et al., 2022), and large quantities of sea ice are injected into the North Atlantic each year through the strait (Reimnitz et al., 1994). The long-term annual average ice outflow in the FS (1935-2014) is approximately 880,000 km^3, accounting for 10% of the sea-ice cover in the Arctic basin (Smedsrud et al., 2017) and the largest portion (90%) of the Arctic sea ice export volume (Sumata et al., 2022; Haine et al., 2015; Serreze et al., 2006). Sea ice is a mixture of ice and brine (Schwerdtfecer, 1963), which gradually melts during outward transport. This process affects freshwater exchange and energy transport in the North Atlantic, which may alter the convective overturning of water masses and thermohaline circulation processes (Aagaard and Carmack, 1989). In addition, for shipping planning and scientific research, the progression of polynyas and lead is heavily influenced by SID (Wagner et al., 2021). Therefore, understanding SID in the FS is crucial to recognizing how sea ice changes in the Arctic and appreciating the connection between the polar regions and the outside world.

With the launch of many remote sensing satellites and the development of remote sensing technology, remote sensing satellite data have become a major data source for SID retrieval (Kwok, 2010). Satellite data can be retrieved to obtain a spatially and temporally continuous sea ice drift field, which helps researchers to better evaluate the sea ice variation in the Arctic and provides a basis for climate forecasting and ship route planning. At present, the primary data used in SID retrieval are radiometers, scatterometers, synthetic aperture radar (SAR) and optical imagers. SID Products based on radiometers and scatterometers often yield lower-resolution due to the inherent characteristics of the sensors. Low resolution SID products exhibit large errors on ice drift speed in the FS region (Hwang, 2013). OSI SAF scatterometer and radiometer based SID products are available for many years over FS region, however, the products tend to have time intervals greater than one day. Due to the complexity of sea ice dynamics, low temporal resolution SID product may fail to provide accurate sea ice drift patterns. High spatiotemporal resolution SID products are highly valuable for capturing sea ice drift patterns (Johansson and Berg, 2016). SAR images provide high spatial resolution, but radar backscatter is sensitive to liquid water on the sea ice surface, and the accuracy of retrieving SID during melting periods can be hampered (Stern and Moritz, 2002). This disadvantage constrains the application of SAR in retrieving SID. Optical images have a long history of application in geo-parameter retrieval. With many satellites equipped with optical imagery in orbit and optical data having the advantages of wide swath and high resolution, optical imagery can accurately capture the surface roughness and texture characteristics of sea ice. Thus, optical remote sensing data have the potential to retrieve SID in the FS (Petrou and Tian, 2017). While optical imagery has the advantage of high resolution and wide swath, this can also significantly increase the computational effort of the algorithms. To solve this problem, our study applied MCC (maximum cross-correlation) algorithm with improvements for SID retrieval. MCC

https://doi.org/10.5194/egusphere-2023-1927
Preprint. Discussion started: 9 October 2023

has been widely employed in retrieving SID with radiometers and scatterometers as well as SAR (Girard-Ardhuin and Ezraty, 2012; Hollands and Dierking, 2011). However, when it comes to utilizing optical images for SID retrieval, many researchers tend to choose different algorithms in addition to MCC. [Petrou et al.] designed an algorithm based on optical flow to retrieve SID from MODIS (Petrou and Tian, 2017). Nevertheless, due to the absence of buoys in their study area, the accuracy of their algorithm is unevaluated. [Lopez-Acosta et al.] developed a complex ice tracking algorithm specifically designed for retrieving SID in the FS region but requiring multiple MODIS images to generate a complete sea ice drift field (Lopez-Acosta et al., 2019). [Fang et al.] discussed the potential of feature tracking algorithms in enhancing MODIS images for SID retrieval. The accuracy of their result is excellent, but the defect in which feature tracking cannot produce vectors that are widely distributed and uniform in the SID field still unsolved (Fang et al., 2023). [Wang et al.] also designed an ice tracking algorithm to retrieve SID in the marginal ice zone (MIZ), but the algorithm cannot produce an intact SID field (Wang et al., 2021). The European Organization for the Exploitation of Meteorological Satellites (EUMETSAT) uses the MCC algorithm to retrieve SID from AVHRR with a spatial resolution of 20 km and a temporal resolution of 1 day (Dybkjaer, 2018). However, it has been observed that the accuracy of the SID product with AVHRR is not good in s regions like East Greenland, with a Mean Absolute Error (MAE) in speeds reaching 10.40 km/day, even lower than the SID products of radiometer and scatterometer (Wang et al., 2022). In our study, we apply multi-template matching combined with a subpixel estimation algorithm for SID retrieval. The method of multi-template matching achieves a balance between computational efficiency and accuracy, and the subpixel estimation further improves the accuracy of the retrieval results while saving some computational resources. We believe that using MCC with improvements, the MCC algorithm can be effectively utilized for retrieving SID from optical images.

This paper focuses on designing an improved MCC algorithm using Coastal Zone Imager (CZI) of Haiyang-1D (HY-1D) data to retrieve SID in the FS. Moreover, the retrieved results are evaluated by comparing them with SAR-based SID products released by CMEMS and IABP buoy data. As for sea ice motion, the average velocity of the sea ice in Arctic is 0.02 m/s (Colony and Thorndike, 1984), and as the main export of sea ice from the Arctic, the sea ice in the FS can achieve a maximum velocity of 0.5 m/s (Qiu and Li, 2022), which makes retrieving SID of the area more sophisticated. Multiyear ice (MYI) drift from the Arctic basin is intensely fragmented in the central strait by TPD and multiple external forces, which makes the sea ice in the southern part of the FS and on the east coast of Greenland exist as drift ice. The drift ice drifts at a faster rate near the FS compared to sea ice within the Arctic Basin. The sea ice characteristics described above increase the difficulty of accurately retrieving SID. For our study, in comparison with other products, the retrieved SID from CZI images achieves good accuracy in the FS and we also find that the algorithm is able to retrieve SID from drift ice located on the east coast of Greenland using images with short time intervals. In previous studies, a sophisticated method was needed to retrieve the motion of drift ice, and our results indicate that the MCC algorithm with improvements can also accurately retrieve the motion of drift ice in the FS.

The paper is structured as follows. Section II describes the data used in this study, including CZI data, CMEMS SID products and IABP buoy data. Section III details the algorithms used to retrieve SID in our study. Section IV compares the results with

https://doi.org/10.5194/egusphere-2023-1927
Preprint. Discussion started: 9 October 2023

CMEMS SID products and buoy data for validation. Section V discusses the retrieved results. Finally, concluding remarks are provided in Section VI.

2 Data

2.1 HY-1D CZI data

The HY-1D satellite is equipped with the Chinese Ocean Color and Temperature Scanner (COCTS), CZI, Ultraviolet Image (UVI), Satellite Calibration Spectrum, and Automatic Identification System. The revisit period of the CZI is three days, the resolution of the CZI image is 50 m, and the swath of the CZI image is nearly 950 km. CZI possesses four bands（VIR and NIR）, as shown in Table 1. The wide swath and high resolution of CZI give us an opportunity to understand the sea ice motion in the FS in detail. In this paper, SID retrieval is performed using the L1C data from CZI. The CZI images are resampled to 300 m for the algorithm's computational efficiency and the resolution of the results.

Table 1: Information on HY-1 D CZI data.

Band	Wavelength (μm)	Band name
1	0.42-0.50	Blue
2	0.52-0.60	Green
3	0.61-0.69	Red
4	0.76-0.89	Near Infrared

For the Arctic region, where climate conditions are harsh and sea ice changes rapidly in response to shifts in ocean currents and winds, this is a potentially hazardous factor for shipping and scientific expedition, achieving timely and accurate monitoring of SID is a crucial goal of polar research. The CZI image has the high spatial resolution and wide swath for providing accurate monitoring of SID. In our study, 111 CZI images from March to May 2021 are used to calculate the intersection region (as shown in Fig. 1(a)) to produce the dataset, and forty-eight pairs of images are eventually produced for SID retrieval. Furthermore, to explore the influence of the image time interval on sea ice retrieval, the 48 pairs of image datasets are divided into 16 pairs of hour-level (less than 6 hours) datasets and 32 pairs of day-level (approximately 24 hours) datasets. Fig. 1(b) shows the time interval histogram of image pairs, and Fig. 1(c) plots the outer frame lines of image pairs, where the white borders are the locations of image pairs at the hours-level, and the darker blue borders are the locations of image pairs at the day-level.

https://doi.org/10.5194/egusphere-2023-1927
Preprint. Discussion started: 9 October 2023

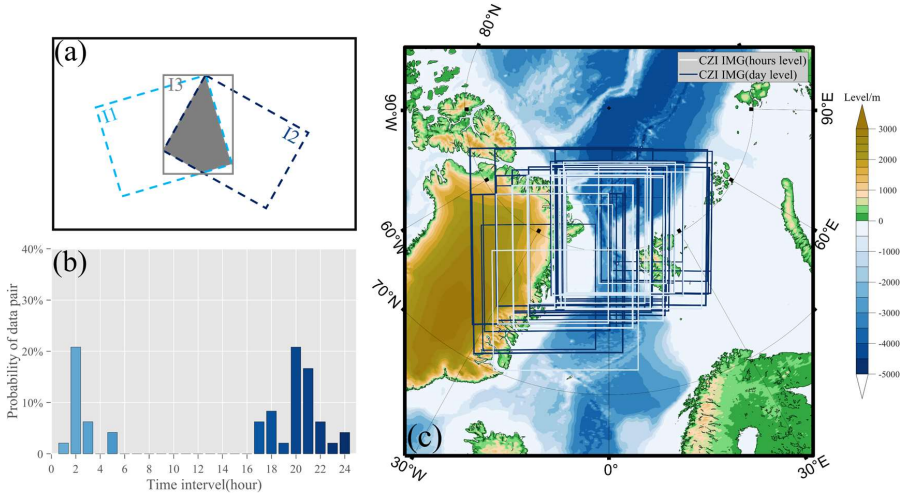

Figure 1: Example showing creation of a clipped image using CZI images (a), time interval histogram of the dataset (b) and location of image pairs (c).

2.2 CMEMS SID product

As the CZI image possesses a high resolution, the SID products retrieved from the scatterometer and radiometer are not comparable for validation. Thus, we choose the SAR-based product for comparison. The Global Ocean-High Resolution SAR Sea Ice Drift is a polar near real-time gridded sea ice drift product produced by the National Space Institute at the Technical University of Denmark (DTU space) (European Union-Copernicus Marine Service, 2015). The data are distributed on the Copernicus Marine Service website. The nominal time interval of each product is 24 hours. The grid resolution of the product is 10 km, and the product includes the North Pole and South Pole (Pedersen et al., 2015). The product has been validated routinely every three months using Woods Hole ice tethered profilers (ITPs). Sea ice drift changes rapidly in the FS, and retrieving SID from images at different times is incompatible. The CMEMS product with more overlap with the time range of CZI images is chosen for comparison.

2.3 IABP buoys

GPS position data from buoys are the most credible data source for the retrieved SID's validation. The International Arctic Buoy Programme（IABP) has deployed a network of drifting buoys in the Arctic to provide data for scientific research (Rigor et al., 2008). IABP has collected over 500 months of data from over 500 buoys deployed in the Arctic. Buoy data collected from IABP are an essential component of Arctic scientific data. These data have been widely used to validate retrieved SID (Hakkinen et al., 2008; Fang et al., 2023). The drift trajectories of the 69 buoys in this paper are shown in Fig. 2 and these drift

https://doi.org/10.5194/egusphere-2023-1927
Preprint. Discussion started: 9 October 2023

trajectories consist of consecutive GPS points. Among of buoys for validation, 33 buoys from MOSAiC are included. Based on the buoys data, 344 matched drift vectors were produced for the retrieved SID's validation.

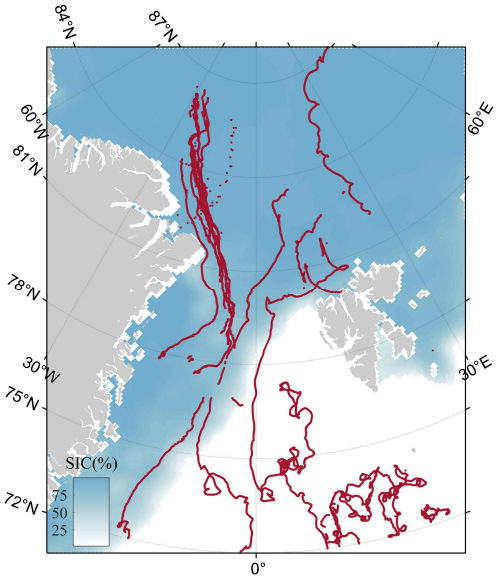

Figure 2: The drifting trajectories of 69 IABP buoys from March to May 2021, SIC (sea ice concentration).

3 Improved SID Retrieval Method in the Fram Strait

The data processing flowchart of this paper is shown in Fig. 3. Although the CZI image has a large swath, a single image can only partially cover the FS. Therefore, mosaicking of the images is necessary. After mosaicking, the intersection area is clipped to generate a set of image pairs. Data enhancement in preprocessing is used to increase the distinction between sea ice and seawater in the image, highlighting the textural details of the sea ice. Data enhancement is indispensable for optical images. Some research has applied data enhancement in preprocessing with optical images (Fang et al., 2023; Lopez-Acosta et al., 2019; Yan et al., 2023). The data enhancement process can aid our algorithm, based on MCC, to retrieve SID more precisely. After preprocessing, the sea ice displacement will be retrieved by multi-template matching and subpixel estimation. Since the optical images are susceptible to some factors, such as clouds and the angle of incidence of the light (Stow et al., 2004), the SID field with noise and low cross-correlation exist in the results, and we design a quality control session to remove the low-quality data from the results. The penultimate step is smoothing and filling to derive an intact SID field. Finally, we validate the results with buoy and CMEMS SID products.

https://doi.org/10.5194/egusphere-2023-1927
Preprint. Discussion started: 9 October 2023

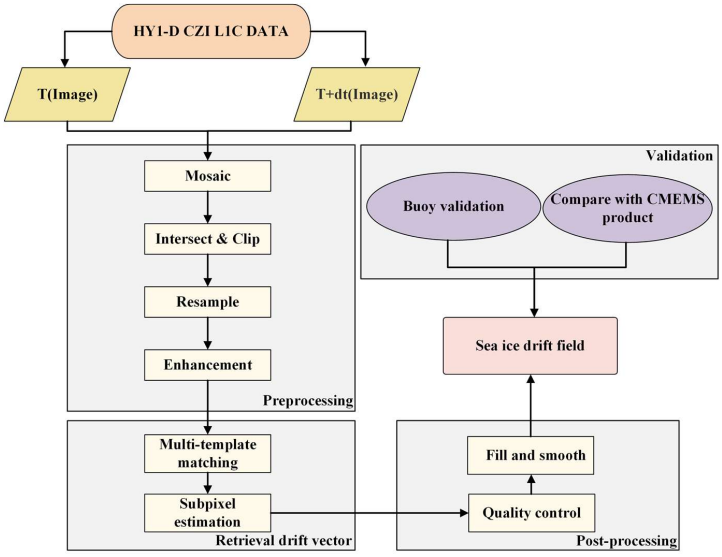

Figure 3: Flow chart of sea ice drift retrieval.

3.1 Data enhancement

Before preprocessing, the resampled image radiance values are converted to grayscale (0-255). Then, the data of different bands are logarithmically stretched separately. After investigating studies that used optical sensors to retrieve SID (Fang et al., 2023), we selected the average of the band 2, 3, and 4 as the input data for the algorithm. Finally, histogram equalization and edge detection are applied to the images. The process and effect of data enhancement are explicitly described as follows.

In the polar regions, the lighting conditions are complex, and some images are captured with a slight solar zenith angle (Stow et al., 2004). These disadvantages could lead to an uneven spatial distribution of image gray values, which affects the retrieval of SID. Logarithmic stretching is an image grayscale transformation that expands the low gray value portion and compresses the high gray value portion (Lupton et al., 2004). Equation (1) is the formula for logarithmic stretching, where r is the gray value of the image and c is the base. The larger the base is, the stronger the emphasis is on the lower gray portions and the stronger the compression of the higher gray portions is. As shown in Fig. 4(a) and (b), applying logarithmic stretching to the image corrects the uneven lighting and enhances the sea ice detail in darker areas.

$$T(r) = c * log(1 + r), \quad (1)$$

In addition to logarithmic stretching, histogram equalization (HE) is also a common method to adjust the grayscale distribution of images (Krutsch and Tenorio, 2011). The adaptive histogram equalization (AHE) algorithm is a variant of histogram equalization (Pizer et al., 1987). It changes the image contrast by calculating the local histogram of the image and then

https://doi.org/10.5194/egusphere-2023-1927
Preprint. Discussion started: 9 October 2023

redistributing the value. This algorithm is an improvement over the traditional HE method, but the disadvantage of AHE is that it introduces noise during grayscale stretching. Currently, contrast limited adaptive histogram equalization (CLAHE) has improved over AHE (Zuiderveld, 1994); therefore, in this study, we chose CLAHE to redistribute the gray value of the image. The change in the image histogram during grayscale transformation is shown in Fig. 4(d). Logarithmic stretching improves the gray value of the image (Fig. 4(b)), and CLAHE enhances the texture and gap feature of sea ice in dense regions (Fig. 4(c)). Cloud cover could lead to a loss of contrast and diminished texture detail, affecting the quality of the retrieval. Edge detection is a method of image enhancement in computer vision (Brooks, 1978). In our study, Sobel edge detection is applied to enhance the texture of sea ice, and we find that edge detection can also remove some of the effects of thin clouds. We will describe this aspect in more detail in the discussion section.

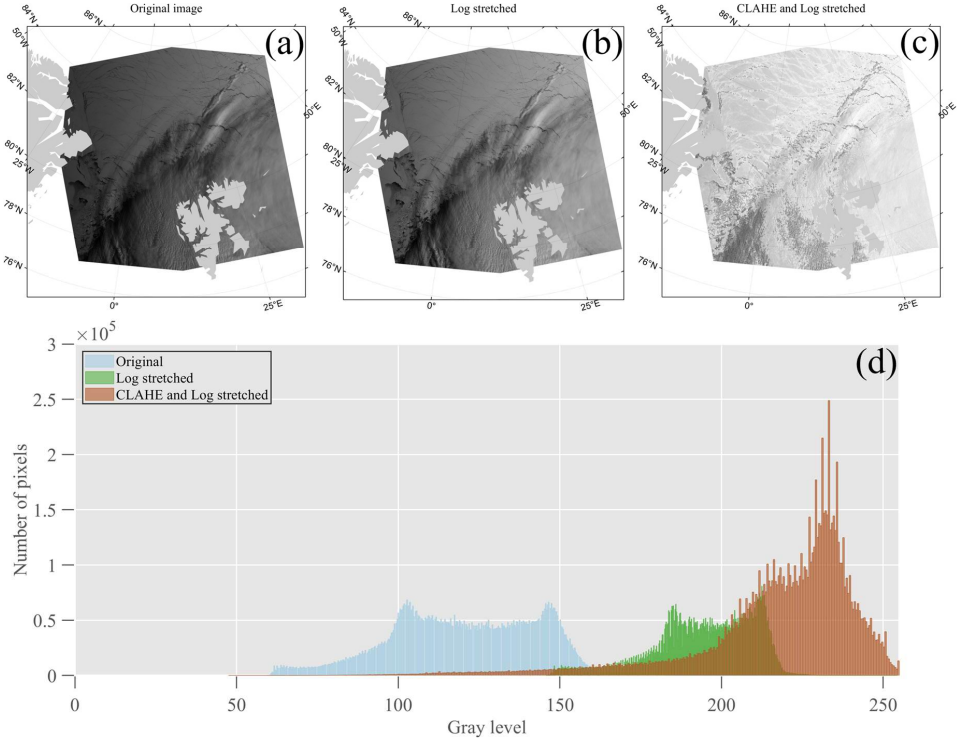

Figure 4: An example of the CZI image (band 2, 3, and 4) before and after data enhancement and their grayscale histogram. (a) is the original image and the color of its histogram is light blue, (b) is the image after logarithmic stretching and the color of its histogram is green, (c) is the image after logarithmic stretching and CLAHE and the color of its histogram is brown, (d) is the grayscale histogram of above images. The date of the image is 07 April 2021, 07:16:35 LT.

https://doi.org/10.5194/egusphere-2023-1927
Preprint. Discussion started: 9 October 2023

3.2 Sea ice drift retrieval

3.2.1 Multi-template matching

The traditional template matching retrieval of SID requires searching a range of images to determine the location with the largest correlation coefficient, and this step could consume a considerable amount of time. Multi-template matching can be performed at different template size, ranging from coarse resolution to fine resolution, to reduce calculation time while ensuring accuracy (Wang et al., 2008). As multi-template matching accounts for the efficiency of the calculation while guaranteeing accuracy, this method is chosen in the study to retrieve SID. As shown in Fig. 5, the time cost of multi-template matching for the 48 data pairs designed in this study is under 150 s, and the average number of pixels in the retrieved images is 5,208,298 pixels. This result indicates that multi-template matching has a high computational efficiency for wide-swath images. In addition, cross-correlation calculations are required during template matching, and calculations are slow (Thielicke and Stamhuis, 2014) in the spatial domain and cannot yield a correlation matrix of roughly equal size to the template. Therefore, we calculate the correlation in the frequency domain to save computational resources.

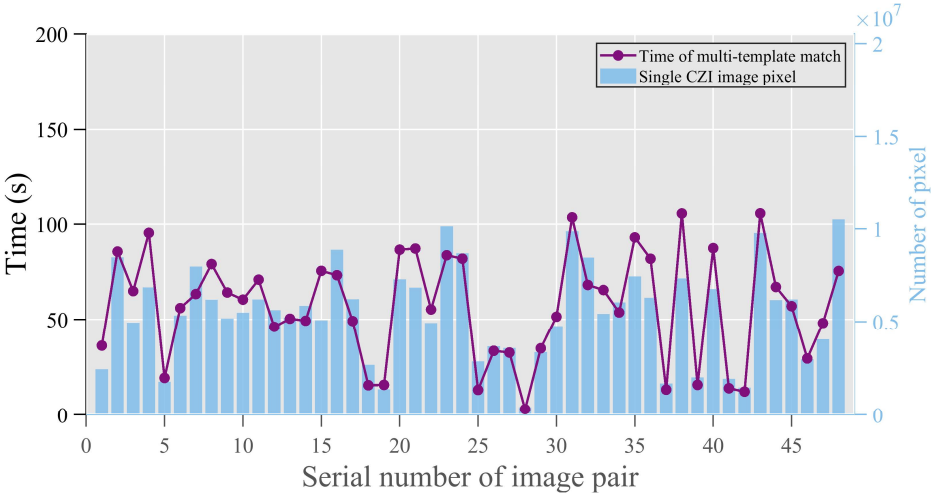

Figure 5: Relationship between multi-template match time cost and image size.

3.2.2 Subpixel estimation

The method of locating the maximum peak of the correlation coefficient is an essential factor in ensuring the accuracy of the MCC. The integer displacements of the two templates can be determined directly from the peak positions of the correlation matrix. However, this approach may introduce quantization errors, and the difference in the minimum displacements will be multiples of the image resolution (Lavergne et al., 2010). To address this issue, subpixel precision refinement of peak positions with the biquadratic surface fitting method has been proposed to mitigate quantization errors (Kwok et al., 1998), but [Thomas

https://doi.org/10.5194/egusphere-2023-1927
Preprint. Discussion started: 9 October 2023

et al.] mentions in their research that subpixel estimates could result in considerable computational costs (Hollands and Dierking, 2011). Therefore, for our study, we have opted for simple Gaussian fitting as a method for subpixel estimation since it strikes a balance between computational efficiency and accuracy (Thielicke and Stamhuis, 2014).

3.3 Quality control

After performing multi-template matching and subpixel estimation, the retrieved SID field is presented in Fig. 6(a). However, due to the influence of clouds and seawater, certain areas of the obtained displacement field exhibit a low confidence level. The MCC algorithm may erroneously extract SID vectors, and it is necessary to filter those erroneous vectors (Haarpaintner, 2006; Lavergne et al., 2010). Therefore, we employ a series of methods to ensure the quality of the displacement field. By applying these quality control measures, consistency within the displacement field is ensured while eliminating erroneous drift fields present in open water regions. Subsequent sections provide detailed descriptions of these quality control methods.

3.3.1 Cross-correlation value and its derived parameters filter

The magnitude of the cross-correlation in the MCC method serves as an indicator of result quality (Haarpaintner, 2006). It represents the correlation between two templates, making it a suitable parameter for initial result quality control. Additionally, we employ two parameters derived from the cross-correlation matrix to further ensure result quality. In the selection of peaks, incorrect peaks are observed near the peaks and can also be labeled subpeaks. Measuring the ratio of peaks to subpeaks provides a measure of the 'uniqueness' of the real peak. Furthermore, comparing the mean of the correlation coefficient matrix with the peaks provides a measure of the signal-to-noise level of the peaks. Two parameters, PMR (peak mean ratio) (Eq. 2) and PSR (peak second ratio) (Eq. 3) (Dybkjaer, 2018; Van Wyk de Vries and Wickert, 2021), are used to measure the quality of the result.

$$PMR = \frac{C_{peak}}{\text{mean}(\text{abs}(C_{all-corr})}, \quad (2)$$

$$PSR = \frac{C_{peak}}{C_{subpeak}}, \quad (3)$$

In the above equation, C_{peak} is the peak of cross-correlation, $C_{all\text{-}corr}$ is the sum of the cross-correlation value, and $C_{subpeak}$ is the second peak of cross-correlation. Fig. 6(c) shows the results using neighborhood filter and co-filtering with the cross-correlation value and its derived parameters filter. Compared to Fig. 6(b), which solely employs neighborhood filter, incorporating the cross-correlation and derived parameters filter effectively eliminates erroneous outcomes within open water regions.

https://doi.org/10.5194/egusphere-2023-1927
Preprint. Discussion started: 9 October 2023

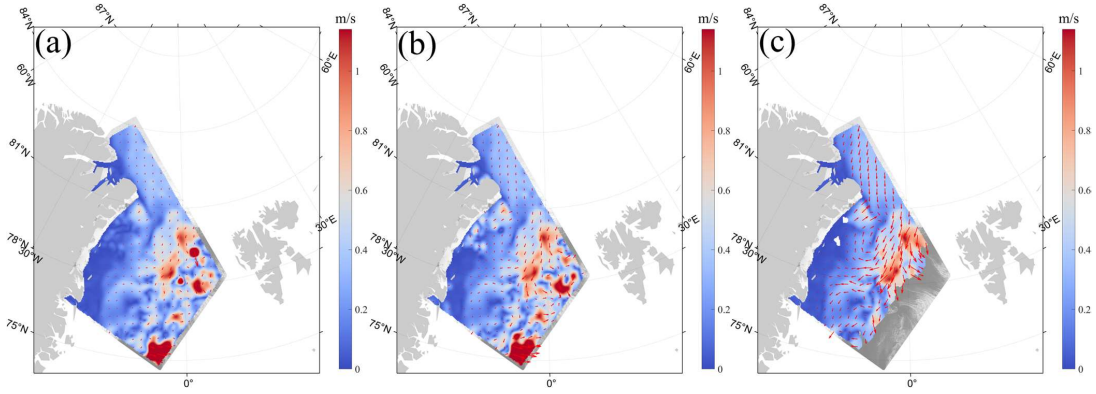

Figure 6: An example of quality control applied to sea ice drift retrieval. (a: SID with no quality control, b: SID after neighborhood filter (only), c: SID after using neighborhood filter and cross-correlation value and its derived parameters filter).

3.3.2 Neighborhood filter

Neighborhood filtering is commonly employed for postprocessing retrieved SID data by removing abrupt values indicative of incidental anomalous drifts that deviate from continuous sea ice movement patterns (Hyun and Kim, 2017; Girard-Ardhuin and Ezraty, 2012). In our study, two window sizes are designed for neighborhood filtering. Fig. 6(b) shows the results of using neighborhood filtering only. Compared to Fig. 6(a), the neighborhood filtering removes the regions (upper part of the image) with significant velocity differences in the SID, but the method is not comprehensive. Jointing the cross-correlation value and its derived parameters filter is necessary to control the quality of the results.

3.4 Fill and smooth

The utilization of correlation coefficients and their derived parametric filtering and neighborhood filtering enhances the quality of the results, but it also introduces blank values appearing in the results. Given the sea ice is spatially distributed continuously, neighboring values are employed to fill in these gaps and smoothen the outcomes during the final step of retrieving sea ice drift. Consequently, robust SID fields are generated.

4 Results and validation

In this study, SID in the FS with a resolution of approximately 4 km is retrieved from the CZI image dataset. These results are categorized into day-level and hours-level results based on the image time interval and compared to IABP buoys and the CMEMS SID product, respectively.

https://doi.org/10.5194/egusphere-2023-1927
Preprint. Discussion started: 9 October 2023

4.1 Comparison of results with CMEMS products

4.1.1 SID with day-level time intervals

In this study, higher-resolution SID fields are retrieved using CZI with a resolution of approximately 4 km. These SID products based on radiometer or scatterometer data cannot be compared to SID in this study due to the resolution difference. Therefore, the SAR-based sea ice drift product (10 km) published by CMEMS is selected for comparison. The reliability of the CMEMS product has been verified in the released user manual (European Union-Copernicus Marine Service, 2015).

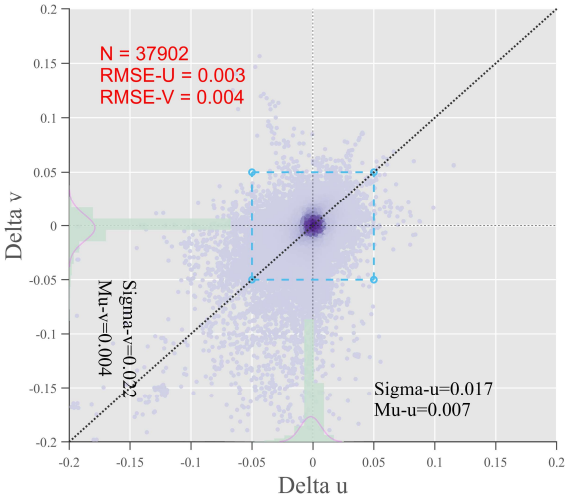

Figure 7: The U-V difference between the retrieved SID (day-level) and CMEMS SID. The histograms on the x and y axes show the distribution of differences in the U and V directions, and the pink curves fit the histograms. The dashed blue box is 0.05 m/s, and the color shading reflects the density of the scatter distribution.

Fig. 7 shows the U-V difference between the SID obtained by CZI and CMEMS products, totaling 37,902 matched points. The U-V differences between the retrieved SID and the CMEMS products are relatively slight at a time interval of approximately 24 hours (day-level), with most of the U-V differences being less than 0.05 m/s and the majority of the scatter distributed in the plot's center. The RMSEs of U-V for the SID and SAR products is 0.003 m/s and 0.004 m/s, respectively. There is a strong correlation between the CMEMS SID and the recovered SID, which is shown by the histograms and accompanying fitted curves with a normal distribution on the X and Y axes.

https://doi.org/10.5194/egusphere-2023-1927
Preprint. Discussion started: 9 October 2023

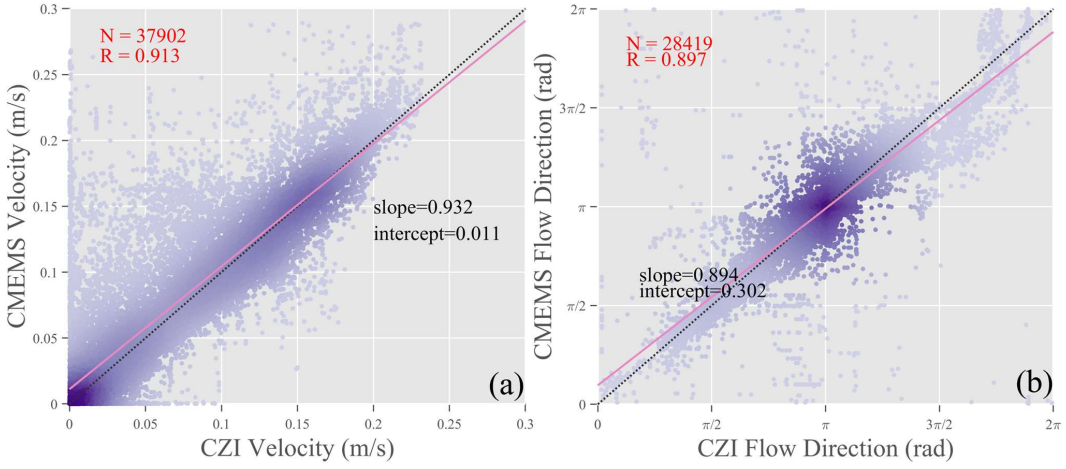

Figure 8: The difference in velocity (a) and flow direction (b) between the retrieved SID (day-level) and CMEMS SID. The dashed line denotes the identity line, and the pink line denotes the fit line.

The velocity difference between the retrieved SID and the CMEMS SID, which includes a total of 37,902 matched points, is illustrated in Figure 8(a). The retrieved SID demonstrates superior velocity correlation with CMEMS SID, as indicated by a high correlation coefficient of 0.913 and a fitted line that closely aligns with the ideal line. The statistical information on the difference between the retrieved SID and CMEMS SID is presented in Table 2, revealing RMSE values of 0.003 m/s for U component, 0.004 m/s for V component, and 0.005 m/s for overall velocity respectively. These slight differences reflect the consistency between the retrieved SID and CMEMS SID.

Previous studies have shown that CMEMS products have a maximum velocity of approximately 0.4 m/s in the FS (Qiu and Li, 2022). In our study, a small template is chosen considering the retrieved SID resolution, which results in the velocity magnitude of the retrieved SID being less than 0.25 m/s. However, compared the results with the CMEMS SID, only a relatively small portion of the velocity of the retrieved SID is greater than 0.25 m/s (Fig. 7(a)). Therefore, the size of the template for our study is capable of retrieving the sea ice drift in the FS, considering the resolution of the results. The effect of template size on retrieving SID will be explored in future research.

Fig. 8(b) shows the flow direction difference between the retrieved SID and CMEMS SID using a total number of 28419 matched points. The correlation of the flow direction between the retrieved SID and CMEMS SID is excellent with a correlation coefficient of 0.897. The statistical information on the difference in flow direction between the retrieved SID and CMEMS is shown in Table 2, with the RMSE of the flow direction being 0.008 rad.

https://doi.org/10.5194/egusphere-2023-1927
Preprint. Discussion started: 9 October 2023

Table 2: Validation of the retrieved SID (day-level) with CMEMS SID.

Delta	Number of match point	BIAS	MAE	STD	RMSE
U (m/s)	37902	-0.003	0.009	0.017	0.003
V (m/s)		-0.004	0.013	0.024	0.004
Velocity (m/s)		-0.005	0.014	0.027	0.005
Flow direction (rad)	28419	0.009	0.147	0.369	0.009

Regarding the flow direction, the sea ice flow direction in the FS predominantly flows from "π/2" to "3π/2" (with the positive y axis as the starting point in polar stereographic projection). The most abundant flow direction is "π", which indicates the southern part of the FS. In the comparison of flow directions, it is observed that the shelf ice on the east coast of Greenland exhibits slower velocities (less than 500 m/day) than the drift ice in the strait (greater than 5000 m/day). Due to potential inaccuracies associated with short sea ice displacements, a shelf ice mask has been established to exclude slow-moving shelf ice. The impact of sea ice displacement on retrieval accuracy will be analyzed in the discussion section.

4.1.2 SID with the hours-level time interval

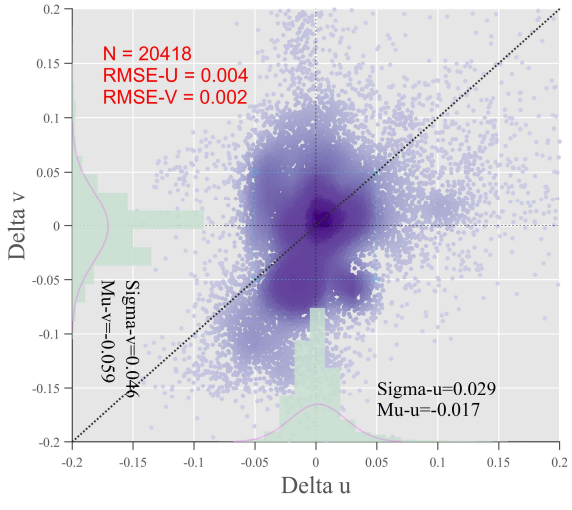

Figure 9: The U-V difference between retrieved SID (hours-level) and CMEMS SID. The histograms on the x and y axes show the distribution of differences in the U and V directions, and the pink curves are a fit to the histograms. The dashed blue box is 0.05 m/s, and the color shading reflects the density of the scatter distribution.

https://doi.org/10.5194/egusphere-2023-1927
Preprint. Discussion started: 9 October 2023

Fig. 9 shows the difference in U-V between the retrieved SID and CMEMS SID for time intervals of less than 6 hours (hours-level), totaling 20,418 matched points. The scatter distribution of U-V differences in Fig. (8) appears significantly more dispersed than that in Fig. (7), suggesting notable disparities between the retrieved SID at the hours-level and the CMEMS SID. The differences may be associated with the spatial and temporal variabilities in sea ice motion and will be explicitly analyzed in the discussion section.

4.2 Comparison of results with IABP buoys

4.2.1 SID with day-level time intervals

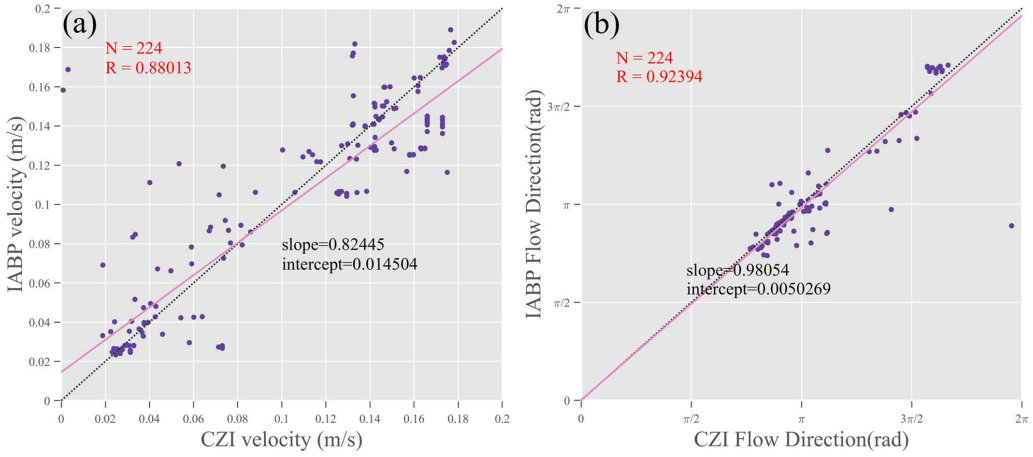

Figure 10: Comparisons between retrieved SID (day-level) and IABP buoys in the velocity magnitude (a) and direction (b); the dashed line denotes the identity line, and the pink line denotes the fit line.

The GPS positioning information of the buoys serves as a crucial reference for validating the accuracy of the retrieved SID. Fig. 10 illustrates the difference in velocity (a) and direction (b) between the results of the day-level and buoys measurements, with a total of 224 matched points. The correlation coefficient between the retrieved SID and the buoy vector for velocity is approximately 0.880, while it is approximately 0.924 for flow direction. With the time interval of images being approximately 24 hours (day-level), there is a strong correlation between the retrieved SID and the buoy vector.

Table 3 presents the statistics of the retrieved SID at the day-level and the buoy measurements, indicating a bias value of approximately 0.004 m/s and an RMSE value of approximately 0.027 m/s for velocity, as well as a bias value of approximately 0.057 rad and an RMSE value of approximately 0.313 rad for flow direction.

https://doi.org/10.5194/egusphere-2023-1927
Preprint. Discussion started: 9 October 2023

Table 3: Validation of the retrieved SID (day-level) with IABP buoys.

Delta	Number of match point	BIAS	MAE	STD	RMSE
Velocity (m/s)	224	0.004	0.017	0.026	0.027
Flow direction (rad)		0.057	0.143	0.308	0.313

4.2.2 SID with the hours-level time interval

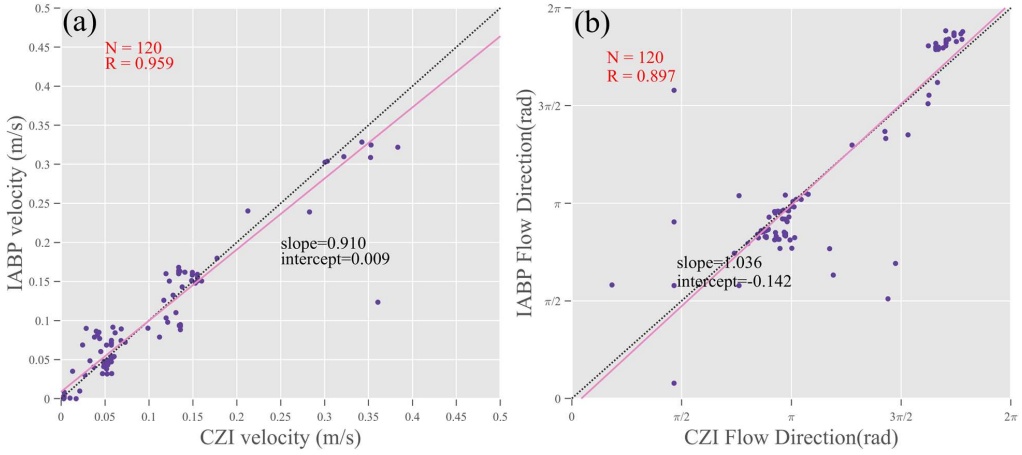

Figure 11: Comparisons between retrieved SID (hours-level) and IABP buoys in the velocity magnitude (a) and direction (b); the dashed line denotes the identity line, and the pink line denotes the fit line.

Fig. 11 shows the difference in velocity (a) and direction (b) between the results of the hours-level and buoy measurements, with a total of 120 matched points. The correlation coefficient of velocity between the retrieved SID and the buoy vector is 0.924, and the correlation coefficient of flow direction between the retrieved SID and the buoy is 0.897. When the time interval of the images is less than 6 hours (hours-level), there is a satisfactory correlation between the retrieved SID and the buoys' vector.

Table 4 provides the statistics of the retrieved SID at the hours-level and the buoy vector, revealing negligible bias values (~0 m/s) along with an RMSE value of 0 .022 m/s for velocity; similarity, there exists the bias value of 0.011 and the RMSE of 0.613 rad for flow direction. [Wang et al.] evaluate eleven satellite SID products over the East Greenland with buoy data and found that the MAEs of velocity for these products are 0.016-0.120 m/s and the MAEs of direction are 0.300-0.973 rad (Wang

https://doi.org/10.5194/egusphere-2023-1927
Preprint. Discussion started: 9 October 2023

et al., 2022). Combined with Table 4 and Table 5, it can be seen that the velocity and direction MAEs of our results are significantly smaller than those of products based on radiometers and scatterometers.

Table 4: Validation of the retrieved SID (hours-level) with IABP buoys.

Delta	Number of match point	BIAS	MAE	STD	RMSE
Velocity (m/s)	120	0.000	0.017	0.022	0.022
Flow direction (rad)		0.011	0.371	0.634	0.631

5 Discussion

5.1 Analysis of the differences between the retrieved SID and CMEMS products

5.1.1 Comparison of each retrieved SID and CMEMS SID

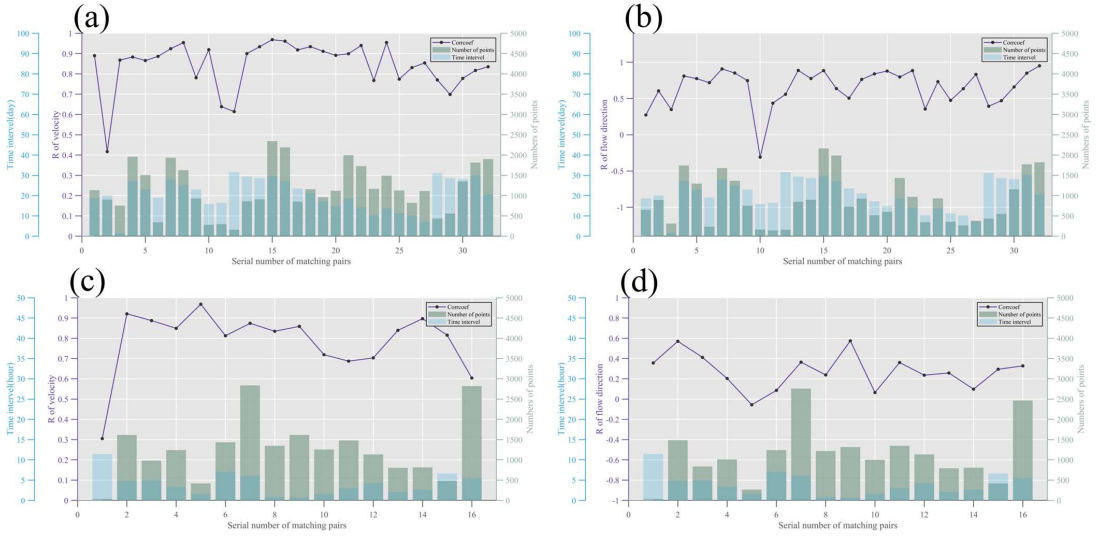

Figure 12: The correlation coefficient between the retrieved SID and the CMEMS SID product, (a), (b): the correlation coefficient between the retrieved SID (day-level) and CMEMS SID in velocity and flow direction. (c), (d): the correlation coefficient between retrieved SID (hours-level) and CMEMS SID in velocity and flow direction. The green histogram (right axis) shows the number of

https://doi.org/10.5194/egusphere-2023-1927
Preprint. Discussion started: 9 October 2023

retrieved SID and CMEMS SID matched points, and the blue histogram (the first left axis) shows the time interval between retrieved SID and CMEMS SID input images.

The statistics of the retrieved SID results and the CMEMS SID product are analyzed in section 4. This section compares the retrieved SID results with the corresponding CMEMS SID product in chronological order. Fig. 12(a) shows the velocity correlation coefficient curve between the day-level results and the CMEMS SID product. Most of the correlation coefficients are greater than 0.7. The 11th and 12th data pairs, on the other hand, have correlation coefficients that are much lower because there are significantly fewer matched points (less than 500) involved. The correlation coefficient of the 2nd data pair is much lower than that of the other data pairs due to the dense clouds in the CZI images, which affects the final retrieval results. Fig. 12(b) shows the correlation coefficient curve of the flow direction between the day-level results and the CMEMS SID product. The correlation coefficient of the 10th pair is negative and considerably different from the others due to the fact that there are less matches in this pair (less than 500). Additionally, the retrieved SID is located on the northeast coast of Greenland. The region is where the TPD and the Greenland's coast meet, and the sea ice movements in the region is unpredictable. Sea ice movement in the area is highly variable due to the influence of winds and other forcing. This finding reveals that interactions between sea ice in the northern FS, where MYI congregates, can drastically affect the flow direction of SID. According to the CMEMS SID product and our results, sea ice interactions cause the flow direction of SID in the northern half of the FS to be more irregular than in the center part of the Strait. Fig. 12(c) shows the velocity correlation coefficient curve between the hours-level results and the CMEMS SID product. The significantly lower correlation coefficient of the 1st pair of data can be attributed to the fact that there aren't enough matched points (less than 200). Fig. 12(d) shows the correlation coefficient curve of the flow direction between the results at the hours-level and the CMEMS SID product. The correlation between the result at the hours-level and the CMEMS SID product in the flow direction is worse by comparing (b) and (d).

https://doi.org/10.5194/egusphere-2023-1927
Preprint. Discussion started: 9 October 2023

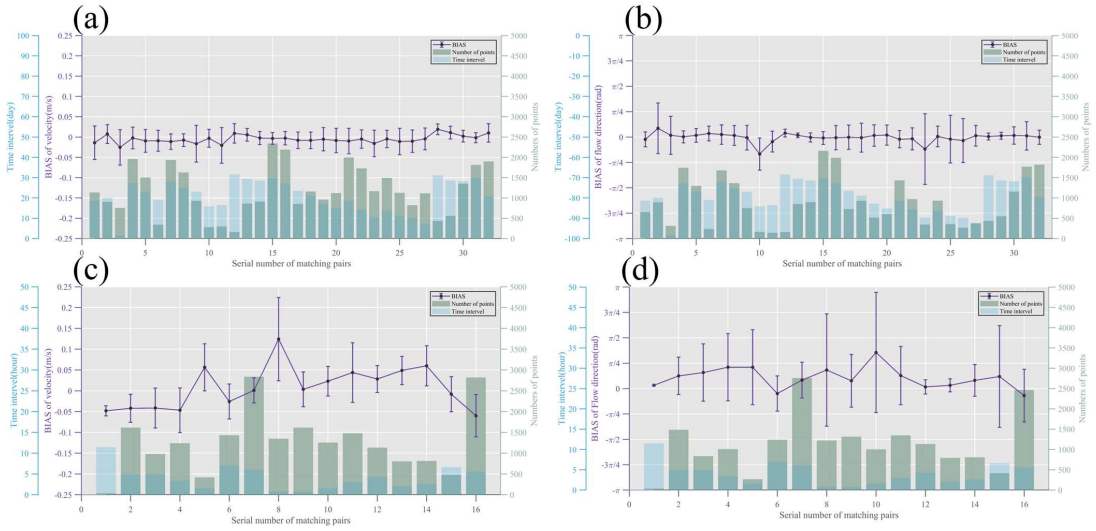

Figure 13: The bias and standard deviation between the retrieved SID and the CMEMS SID, (a), (b): the bias between retrieved SID (day-level) and CMEMS SID in velocity and flow direction. (c), (d): the bias between retrieved SID (hours-level) and CMEMS SID in velocity and flow direction. The green histogram (right axis) shows the number of retrieved SID and CMEMS SID matched points, and the blue histogram (the first left axis) shows the time interval between retrieved SID and CMEMS SID input images.

The difference and standard deviation of velocity between the day-level data and the CMEMS SID product are shown in Fig. 13(a). The velocity bias of the two datasets is less than ± 0.05 m/s, demonstrating a high degree of consistency. When the time interval is large (12th and 28th pairs) or there are fewer matched points (3rd, 10th, 11th and 13th pairs), the deviation and standard deviation of our results and CMEMS SID products become greater. Fig. 13(b) shows the deviation and standard deviation of the flow direction between the day-level results and the CMEMS SID product. The deviation in the flow direction is slight. However, when there are fewer matched points (3rd, 10th and 23rd pairs), the deviation and standard deviation of the flow direction become larger. Fig. 13(c) shows the velocity deviation and standard deviation between the hours-level results and the CMEMS SID product. Although most of the biases are smaller than 0.15 m/s, the velocity bias is significantly more substantial than the day-level data. The variation and standard deviation of the flow direction between the results at the hours-level and the CMEMS SID product are shown in Fig. 13(d). By comparing (a), (b) and (c), (d) in Fig. 13, the day-level results are much less divergent from the CMEMS SID product.

5.1.2 Analysis of the difference

The day-level results compared to the CMEMS SID product are presented in Figs. 7 and 8, revealing the slight difference in U, V, velocity, and flow direction between them. Table (2) statistics also illustrate the minute differences between our results and the CMEMS SID products. However, Fig. 12 shows a significant difference between the hours-level results and the

https://doi.org/10.5194/egusphere-2023-1927
Preprint. Discussion started: 9 October 2023

CMEMS product. The retrieval methods used in our study differ slightly from those of the CMEMS SID products, but both algorithms are based on the MCC. The discrepancy may be attributed to either the time interval of SAR images used in the CMEMS SID product or the time interval between the images used by the two SID results.

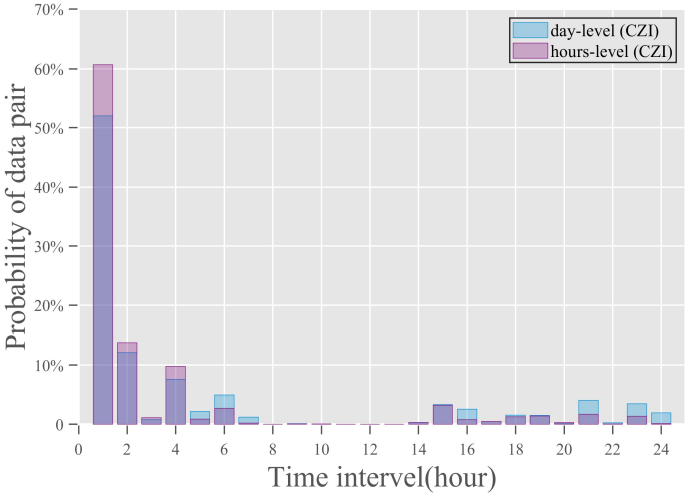

Figure 14: The time interval of SAR images used by the CMEMS SID product.

Fig. 14 shows the time interval of SAR images used for the CMEMS SID products. The blue histogram represents the time interval of the SAR images of the CMEMS SID product, which is used for the comparison with the day-level results, and the purple histogram represents the time interval of the SAR images of the CMEMS SID product, which is used for the comparison with the hours-level results. Fig. 14 shows that the blue and purple histogram distributions are nearly identical. Most SAR image time intervals used in CMEMS SID products are less than 6 hours, and only a few are approximately 20 hours. The consistent distribution trend of the two kinds of histograms indicates that the time intervals of the SAR images used by the CMEMS SID products are basically the same. The distribution of the two histograms explains that the difference between the retrieved results and the CMEMS SID products is not relevant to the time interval of the SAR images used.

https://doi.org/10.5194/egusphere-2023-1927
Preprint. Discussion started: 9 October 2023

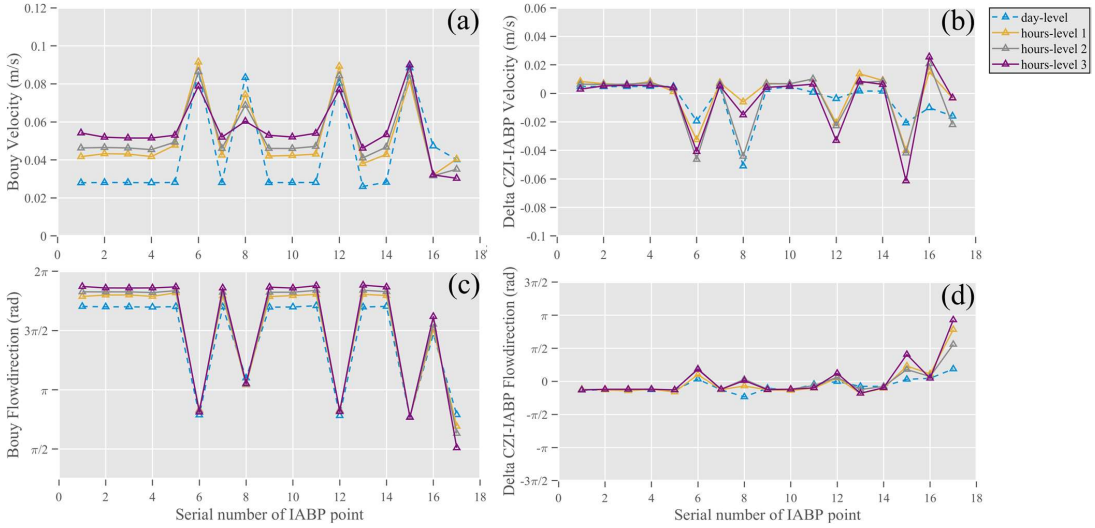

Figure 15: The buoy velocity (a) and flow direction (c) and the difference (velocity (b), flow direction (d)) between the retrieved SID and buoys.

We attribute the difference between the hours-level results and CMEMS SID product to the temporal and spatial variabilities in sea ice motion. Fig. 15(a) and (c) show the variation in velocity and flow direction of 17 different buoys at different time intervals. The day-level CZI pair date is 06 April 2021, 06:10:12 LT and 07 April 2021, 07:16:35 LT. The first hours-level CZI pair date is 06 April 2021, 06:10:12 LT and 06 April 2021, 09:29:35 LT, the second hours-level CZI pair date is 06 April 2021, 06:10:12 LT and 06 April 2021, 11:10:03 LT, and the third hours-level CZI pair date is 06 April 2021, 09:29:35 LT and 06 April 2021, 11:10:03 LT. The triangles in Fig. 15(a) represent the velocity of the buoys, and there is a significant difference in velocity between the day-level buoys and the hours-level buoys. The difference between hours-level buoys is less than the difference between hours-level buoys and day-level buoys, but the difference still exists. The same trend is also found in the flow direction shown in Fig. 15(c). Fig. 15(b) and (d) show the difference in velocity and flow between our results and the buoys, and the day-level result had a smaller difference with the buoys. Additionally, different buoys showed differences from our results, which are related to the location where the buoys are deployed.

https://doi.org/10.5194/egusphere-2023-1927
Preprint. Discussion started: 9 October 2023

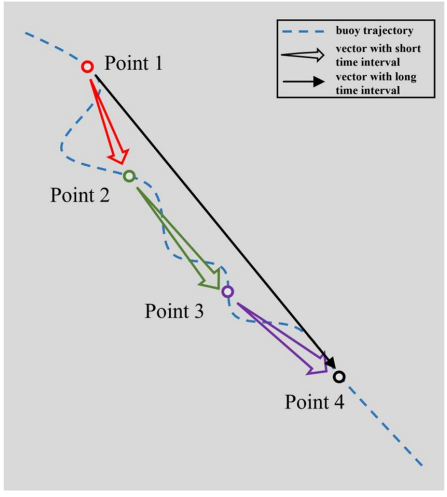

Figure 16: Illustration of SID vector retrievals with different time intervals.

The spatial and temporal variabilities in the buoys and the comparison with our results suggest that SID has large spatial and temporal variability. As shown by the colorful arrows in Fig. 16, there is a large variability in velocity and flow direction when SID is retrieved using images with short time intervals. When the drift vectors retrieved at longer intervals are compared with those retrieved at shorter intervals, some differences are noted. This result is a consequence of the spatial and temporal variability in SID. When comparing the drift vectors retrieved with two different short time intervals, in some extreme situations, a large difference will be presented due to the spatial and temporal variability in sea ice. The variability in SID is more complex and unpredictable on small time scales. The complex spatial and temporal variability in SID explained the discrepancy between the results of this study and the CMEMS SID product.

Despite the spatial and temporal variability in sea ice motion, it is still possible to validate our retrieved results using the CMEMS SID product which remains comparable for this purpose. Furthermore, as long as a sufficiently large time interval is employed, the impact of SID variability diminishes resulting in consistent drift trends being observed. Utilizing SID products for evaluating retrieved results remains valid while providing valuable references through consistency ratings and differences obtained during such comparisons.

5.2 The effect of different time intervals on retrieving SID

Section 5.1 discusses the consistency and discrepancy between the results of this study and the CMEMS SID product, while revealing the spatial and temporal variability in SID. In this section, we explore the impact of different time intervals on retrieving SID by analyzing validation results from the buoys and the statistics of the quality control parameters. The time interval of CZI images is a critical factor in accuracy of retrieving SID. On one hand, the process of detailed SID could be

https://doi.org/10.5194/egusphere-2023-1927
Preprint. Discussion started: 9 October 2023

tracked by using images with short time intervals; on the other hand, SID retrieval from images with longer time interval images provides more stable results. Therefore, it is crucial to determine an appropriate time interval for retrieving SID in the FS.

Section 3.3 describes the three parameters used for quality control: R, PMR and PSR. Table 5 presents the statistics of these parameters at different time intervals over the regions that retained valid SID vectors after quality control and neighborhood filtering. As seen from the mean values, each quality control parameter for the hours-level results is more significant than for the day-level results, which indicates that the hours-level results possess higher quality. However, the standard deviation of the quality control parameters is the opposite. The standard deviation of the quality control parameters for the day-level results is smaller than that for the hours-level results. The statistics indicate that the day-level results remain relatively stable despite having slightly poorer quality.

Table 5: Statistics of quality control parameters at different time intervals.

Parameter	MEAN	STD	Type
R	0.372	0.199	day-level
	0.473	0.225	hours-level
PMR	9.338	4.857	day-level
	13.262	6.198	hours-level
PSR	1.620	0.838	day-level
	2.016	0.980	hours-level

In the comparison with the buoys, the correlation of the results at the day-level is slightly lower than that at the hours-level in terms of velocity. In terms of flow direction, the correlation of the day-level results is slightly higher than that of the hours-level results. The retrieval of images at the day-level is first confronted with the effects of large drift distances, wind, sea ice melt, sea ice break-up, light variations, clouds, etc. Therefore, the velocity accuracy of the day-level results is lower than that of the hours-level results. In the flow direction retrieval, the accuracy of the day-level results is better than that of the hours-level results, which might be relevant in the method of MCC to retrieve the flow direction. When the MCC algorithm retrieves vectors with shorter displacements, a smaller deviation can lead to a larger bias in the flow direction. The trends are also supported by statistical parameters in Tables 3 and 4.

In our study, the dataset is divided into two groups according to the image time interval. In comparison with the buoys, the results of both datasets achieved excellent accuracy. After comparison, we believe that using image pairs with shorter time intervals yields results with high quality but with the disadvantage that the stability of the SID will be poor. According to the accuracy of the day-level dataset, we also believe that retrieving using image pairs with greater time intervals (greater than 6 hours) will provide better results. Our suggestion on time intervals is shorter than the thesis of Qiu, Qiu suggest uses SAR images with about 20 hours to retrieve SID in the FS from January to June (Qiu and Li, 2022). We attribute the divergent conclusions on suitable time intervals due to the limited size of our dataset. In the future studies, we plan to incorporate HY1-

https://doi.org/10.5194/egusphere-2023-1927
Preprint. Discussion started: 9 October 2023

C data and investigate the impact of varying time intervals on SID retrieval, thereby enhancing the comprehensiveness of our research.

5.3 Adaptability of edge detection

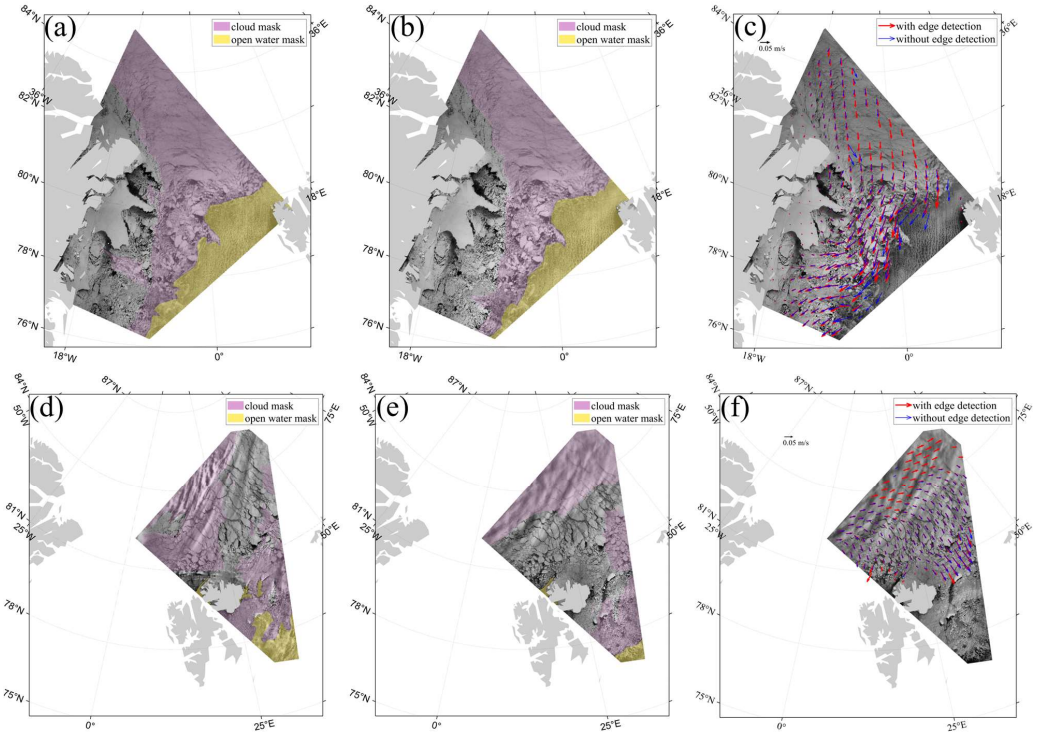

Figure 17: Two examples of retrieving sea ice drift with clouds in an image. Images (a), (b), and (c) are a pair of results, and images (d), (e), and (f) are another pair of results. The arrows in (c) and (f) are diluted for direct viewing, and the open water area in the middle of the sea ice is excluded.

Optical images in retrieving SID can be affected by factors such as clouds, lighting and other variables. In this study, Sobel edge detection is used to enhance the texture of sea ice. Through experimentation, we find that better retrieval results are also achieved for sea ice under thin clouds after using Sobel edge detection. Fig. 17 shows two examples of SID retrieved under thin cloud conditions. The first example has hours-level time interval images for retrieval, with image (a) taken at 27 April 2021, 09:27:33 LT and image (b) taken at 27 April 2021, 11:07:20 LT. The second example has day-level time interval images for retrieval, with image (c) taken at 02 May 2021, 03:20:35 LT and image (d) taken at 03 May 2021, 06:07:37 LT. In the

https://doi.org/10.5194/egusphere-2023-1927
Preprint. Discussion started: 9 October 2023

second example, images (d) and (e) are also covered by thick clouds in addition to thin clouds, which more severely obscure the sea ice texture.

Fig. 17(a) and (b) show clouds and open water in the image by visual interpretation. Fig. 17(c) shows the SID vectors derived from this study, where the vectors with Sobel edge detection in the preprocessing are in red, and the vectors without Sobel edge detection are in blue. A comparison between these two types of vectors reveals a more consistent trend of SID with a homogeneous velocity distribution achieved through the use of Sobel edge detection. This comparison demonstrates that edge detection enhances the retrieval algorithm and illustrates the potential for optical data to retrieve SID under thin cloud conditions. Fig. 17(d), (e) and (f) show another pair of results using CZI images with day-level time intervals. In contrast to the first pair of results, the CZI images (Fig. 17(d), (e)) have many more clouds, and the variation in the distribution of the clouds is very apparent. Comparing the vectors with two different colors, the red vector using edge detection is significantly better, providing results in parts of the thick cloud area. There is a thin cloud distribution in the image's lower right corner, but the algorithm does not give credible results due to the heavily broken sea ice, and our algorithm still needs to be improved to address this situation. Analytically, edge detection strengthens the capability of algorithm to retrieve SID from images with clouds. In addition, Fig. 17 similarly shows the enhancement of the separating capacity of algorithm for open water after applying Sobel edge detection. The red vectors in Fig. 17(c) and (f) are mainly distributed in the sea ice extent. Overall, applying edge detection in preprocessing helped the algorithm to retrieve high-quality SID.

5.4 Factors affecting the accuracy of flow direction retrieval

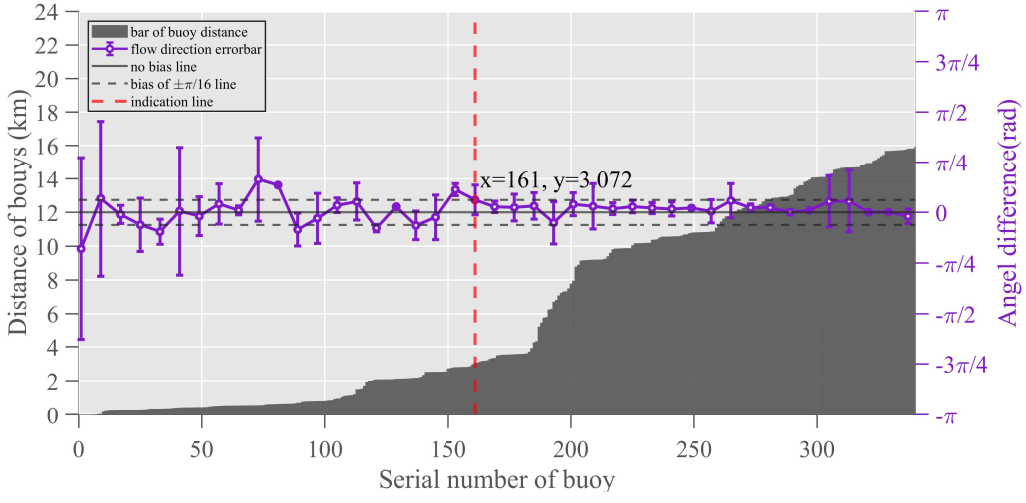

Figure 18: The relationship between the flow direction and the displacement of the buoys.

https://doi.org/10.5194/egusphere-2023-1927
Preprint. Discussion started: 9 October 2023

[Qiu et al.] concluded that the flow direction accuracy of the retrieved SID is associated with the magnitude of the velocity (Qiu and Li, 2022). In our study, when dividing the dataset into hours-level and day-level by time interval for comparison with the buoys, inconsistencies with Qiu's conclusions are found when analyzing the differences in the retrieving flow directions. Compared with the buoy data, the difference in the flow direction of the SID at the day-level is smaller than that of the SID at the hours-level. However, since the coverage areas of both datasets are repetitive, the magnitudes of the SID velocities retrieved from both datasets should be the same. Thus, it is not the velocity magnitude of the SID that affects the accuracy of the retrieving flow direction.

Our study considers that the distance of sea ice displacement affects the accuracy of the flow direction retrieval. Retrieving the precise flow direction at small displacements is challenging, and the time interval needs to be increased to achieve longer sea-ice displacements, although this can also lead to other disadvantages (e.g., clouds, ice breaks) for sea-ice retrieval. Fig. 18 shows the relationship between the drift distance of the buoys and the differences between the retrieved SID and buoy vectors in the flow direction. We generated a total of 344 matched points are and merged every 8 points to calculate the bias and standard deviation. As the buoy displacement increases, the bias and standard deviation of the flow direction decrease, which indicates that the accuracy of the retrieved flow direction is affected by the distance of the sea ice displacement. Larger displacements result in more accurate retrievals but also require longer time intervals with more disadvantageous factors for algorithm performance. Therefore, satisfactory accuracy of flow retrieval can be achieved by controlling the time interval to a displacement of greater than 3 km (approximately 10 pixels in the images), as indicated by the red dashed line in Fig. 18.

6 Conclusion

The retrieval of sea ice drift in the FS is complicated due to the geographic specificity of the region. Sea ice drift within the Arctic basin is dominated by two trends, the BG and TPD. The FS is the outlet of the TPD as well as the intersection of the Atlantic and Arctic. The heavily fragmented nature of sea ice in this strait, coupled with its fast motion, significantly impacts the accurate retrieval of SID. Our method using the multi-template matching and subpixel estimation approach to retrieve SID in the FS produces a promising result. We use 111 views of CZI images to obtain 48 sets of image pairs for analysis purposes. These images are categorized into hours-level and day-level according to the time interval. We found that the day-level results are consistent with the CMEMS product, the hours-level results are slightly different from the CMEMS product due to the spatial and temporal variability in the sea ice motion.

Validation is also carried out using IABP buoys. For velocity, the bias values of the day-level results and hours-level results with the buoys are 0.004 m/s and 0.000 m/s, and the RMSE values of the day-level results and hours-level results with the buoys are 0.027 m/s and 0.022 m/s, respectively. For the flow direction, the bias values of the day-level results and hours-level results with the buoys are 0.057 rad and 0.011 rad, and the RMSE values of the day-level results and hours-level results with the buoys are 0.313 rad and 0.631 rad, respectively. The accuracy of the retrieved SID surpasses that of the SID products obtained by AVHRR.

https://doi.org/10.5194/egusphere-2023-1927
Preprint. Discussion started: 9 October 2023

The SID retrieval method with multi-template matching and subpixel estimation used in our study improves the traditional MCC method. In this study, the reliability and accuracy of the algorithm are verified by comparing the results with buoys. Additionally, in the application of the algorithm, the method of multi-template matching performs satisfactorily in terms of computational speed. Thus, we consider that the method used in this study balances the computational cost and accuracy well. This study verifies the feasibility and validity of using CZI images for SID retrieval in the FS. The spatial resolution of the retrieved SID is 4 km, which is much higher than that of the SID product from scatterometers, radiometers and other optical sensors and is suitable for capturing complex sea ice drift information in the FS. The SID products from scattermeters and radiometers with broader coverage are more suitable for the sea ice mass balance and the assimulation of numerical prediction over the whole Arctic region. This result also illustrates the high potential of the CZI sensor carried by China's HY-1D satellite over the polar regions. At present, the HY-1C and HY-1D satellites have been networked for observation, and the Chinese HY-1 series of satellites will be further utilized to advance polar research. Discontinuation of the Sentinel-1B satellite operation resulted in numerous data gaps on CMEMS SID products from 2022 onwards which severely limited the SID capacity to study long-term sea ice drift in the FS. Through leveraging future expansions of HY1-C data, we anticipate that CZI-retrieved SID will complement CMEMS SID products in forthcoming research, facilitating the utilization of high spatial resolution and high temporal resolution products for studying sea ice dynamics.

Data availability. The HY-1D data are available at http://osdds.nsoas.org.cn/, provided by the NSOAS (last accessed on 30 July 2023). If you have not registered before, you will need to create an account to access the data. Then, you can enter your account and password to log in to the official website to access the HY1-D data. The sea ice drift product is available at ftp://nrt.cmems-du.eu/Core/SEAICE_GLO_SEAICE_L4_NRT_OBSERVATIONS_011_006/DTU-GLO-SEAICE_DRIFT-NORTH-L4-NRT-OBS, and the product is provided by the Copernicus Marine Service Information (CMEMS) (European Union-Copernicus Marine Service, 2015) (last accessed on 30 July 2023). The IABP buoy data are available at f https://iabp.apl.uw.edu/Data_Products/BUOY_DATA/FULL_RESOLUTION_DATA/Arctic/, provided by the International Arctic Buoy Programme.

Author contributions. Data curation, D.L. and L.S.; writing, D.L and L.S.; methodology, D.L. L.S. J.L. T.Z. B.C. S.W. and M.W. ; validation, D.L T.Z. and S.W. ; funding acquisition, L.S and J.L. All authors have read and agreed to the published version of the paper. We dedicate this study to Prof Jianqiang Liu who sadly passed away in the line of work on 25 May 2023. He has played a key role in HY satellite technical configuration and made contributions during the preparation of this manuscript.

Competing interests. At least one of the (co-)authors is a member of the editorial board of *The Cryosphere.*

Acknowledgments. The authors would like to thank the editors and reviewers for their invaluable efforts in improving the paper. The authors would also like to thank the NSOAS, CMEMS, DTU and IABP for providing all the data needed for this paper. The authors would also like to thank GIV creators and PIVLAB crew for providing referential code.

https://doi.org/10.5194/egusphere-2023-1927
Preprint. Discussion started: 9 October 2023

Financial support. The research is funded by the National Key Research and Development Program of China (grant numbers 2021YFC2803300 and 2018YFC1407200), the Impact and Response of Antarctic Seas to Climate Change programme (grant number IRASCC2020-2022-No. 01-01-03), B.C was supported by the European Union's Horizon 2020 research and innovation framework programme (PolarRES project, grant number 101003590).

References

Aagaard, K. and Carmack, E. C.: The role of sea ice and other fresh water in the Arctic circulation, Journal of Geophysical Research: Oceans, 94, 14485–14498, https://doi.org/10.1029/JC094iC10p14485, 1989.

Encyclopedia of Ocean Sciences: http://www.sciencedirect.com:5070/referencework/9780128130827/encyclopedia-of-ocean-sciences, last access: 13 December 2022.

Brooks, M. J.: Rationalizing edge detectors, Computer Graphics and Image Processing, 8, 277–285, https://doi.org/10.1016/0146-664X(78)90054-0, 1978.

Colony, R. and Thorndike, A. S.: An estimate of the mean field of Arctic sea ice motion, J. Geophys. Res., 89, 10623, https://doi.org/10.1029/JC089iC06p10623, 1984.

Cook, B. I., Smerdon, J. E., Seager, R., and Coats, S.: Global warming and 21st century drying, Clim Dyn, 43, 2607–2627, https://doi.org/10.1007/s00382-014-2075-y, 2014.

Dethloff, K., Rinke, A., Benkel, A., Køltzow, M., Sokolova, E., Kumar Saha, S., Handorf, D., Dorn, W., Rockel, B., von Storch, H., Haugen, J. E., Røed, L. P., Roeckner, E., Christensen, J. H., and Stendel, M.: A dynamical link between the Arctic and the global climate system, Geophysical Research Letters, 33, https://doi.org/10.1029/2005GL025245, 2006.

Döscher, R., Vihma, T., and Maksimovich, E.: Recent advances in understanding the Arctic climate system state and change from a sea ice perspective: a review, Atmospheric Chemistry and Physics, 14, 13571–13600, https://doi.org/10.5194/acp-14-13571-2014, 2014.

Dybkjaer, G.: Algorithm Theoretical Basis Document for OSI SAF Medium Resolution Sea Ice Drift Product, 2018.

European Union-Copernicus Marine Service: Global Ocean - High Resolution SAR Sea Ice Drift, https://doi.org/10.48670/MOI-00135, 2015.

Fang, Y., Wang, X., Li, G., Chen, Z., Hui, F., and Cheng, X.: Arctic sea ice drift fields extraction based on feature tracking to MODIS imagery, International Journal of Applied Earth Observation and Geoinformation, 120, 103353, https://doi.org/10.1016/j.jag.2023.103353, 2023.

Finnish Meteorological Institute, Rudels, B., and Carmack, E.: Arctic Ocean Water Mass Structure and Circulation, Oceanog, https://doi.org/10.5670/oceanog.2022.116, 2022.

Girard-Ardhuin, F. and Ezraty, R.: Enhanced Arctic Sea Ice Drift Estimation Merging Radiometer and Scatterometer Data, IEEE Trans. Geosci. Remote Sensing, 50, 2639–2648, https://doi.org/10.1109/TGRS.2012.2184124, 2012.

https://doi.org/10.5194/egusphere-2023-1927
Preprint. Discussion started: 9 October 2023

Haarpaintner, J.: Arctic-wide operational sea ice drift from enhanced-resolution QuikScat/SeaWinds scatterometry and its validation, IEEE Trans. Geosci. Remote Sensing, 44, 102–107, https://doi.org/10.1109/TGRS.2005.859352, 2006.

Haine, T. W. N., Curry, B., Gerdes, R., Hansen, E., Karcher, M., Lee, C., Rudels, B., Spreen, G., de Steur, L., Stewart, K. D., and Woodgate, R.: Arctic freshwater export: Status, mechanisms, and prospects, Global and Planetary Change, 125, 13–35, https://doi.org/10.1016/j.gloplacha.2014.11.013, 2015.

Hakkinen, S., Proshutinsky, A., and Ashik, I.: Sea ice drift in the Arctic since the 1950s, Geophysical Research Letters, 35, https://doi.org/10.1029/2008GL034791, 2008.

Hollands, T. and Dierking, W.: Performance of a multiscale correlation algorithm for the estimation of sea-ice drift from SAR images: initial results, Ann. Glaciol., 52, 311–317, https://doi.org/10.3189/172756411795931462, 2011.

Hwang, B.: Inter-comparison of satellite sea ice motion with drifting buoy data, International Journal of Remote Sensing, 34, 8741–8763, https://doi.org/10.1080/01431161.2013.848309, 2013.

Hyun, C.-U. and Kim, H.: A Feasibility Study of Sea Ice Motion and Deformation Measurements Using Multi-Sensor High-Resolution Optical Satellite Images, Remote Sensing, 9, 930, https://doi.org/10.3390/rs9090930, 2017.

Johansson, A. M. and Berg, A.: Agreement and Complementarity of Sea Ice Drift Products, IEEE J. Sel. Top. Appl. Earth Observations Remote Sensing, 9, 369–380, https://doi.org/10.1109/JSTARS.2015.2506786, 2016.

Krumpen, T., Gerdes, R., Haas, C., Hendricks, S., Herber, A., Selyuzhenok, V., Smedsrud, L., and Spreen, G.: Recent summer sea ice thickness surveys in Fram Strait and associated ice volume fluxes, The Cryosphere, 10, 523–534, https://doi.org/10.5194/tc-10-523-2016, 2016.

Krutsch, R. and Tenorio, D.: Histogram equalization, Freescale Semiconductor, Document Number AN4318, Application Note, 2011.

Kwok, R.: Satellite remote sensing of sea-ice thickness and kinematics: a review, Journal of Glaciology, 56, 1129–1140, https://doi.org/10.3189/002214311796406167, 2010.

Kwok, R., Schweiger, A., Rothrock, D. A., Pang, S., and Kottmeier, C.: Sea ice motion from satellite passive microwave imagery assessed with ERS SAR and buoy motions, J. Geophys. Res., 103, 8191–8214, https://doi.org/10.1029/97JC03334, 1998.

Lavergne, T., Eastwood, S., Teffah, Z., Schyberg, H., and Breivik, L.-A.: Sea ice motion from low-resolution satellite sensors: An alternative method and its validation in the Arctic, Journal of Geophysical Research: Oceans, 115, https://doi.org/10.1029/2009JC005958, 2010.

Li, X., Che, T., Li, X., Wang, L., Duan, A., Shangguan, D., Pan, X., Fang, M., and Bao, Q.: CASEarth Poles: Big Data for the Three Poles, Bulletin of the American Meteorological Society, 101, E1475–E1491, https://doi.org/10.1175/BAMS-D-19-0280.1, 2020.

Lopez-Acosta, R., Schodlok, M. P., and Wilhelmus, M. M.: Ice Floe Tracker: An algorithm to automatically retrieve Lagrangian trajectories via feature matching from moderate-resolution visual imagery, Remote Sensing of Environment, 234, 111406, https://doi.org/10.1016/j.rse.2019.111406, 2019.

https://doi.org/10.5194/egusphere-2023-1927
Preprint. Discussion started: 9 October 2023

Lupton, R., Blanton, M. R., Fekete, G., Hogg, D. W., O'Mullane, W., Szalay, A., and Wherry, N.: Preparing Red-Green-Blue Images from CCD Data, PASP, 116, 133, https://doi.org/10.1086/382245, 2004.

Martin, T. and Augstein, E.: Large-scale drift of Arctic Sea ice retrieved from passive microwave satellite data, J. Geophys. Res., 105, 8775–8788, https://doi.org/10.1029/1999JC900270, 2000.

Maslanik, J., Stroeve, J., Fowler, C., and Emery, W.: Distribution and trends in Arctic sea ice age through spring 2011, Geophysical Research Letters, 38, https://doi.org/10.1029/2011GL047735, 2011.

Pedersen, L. T., Saldo, R., and Fenger-Nielsen, R.: Sentinel-1 results: Sea ice operational monitoring, in: 2015 IEEE International Geoscience and Remote Sensing Symposium (IGARSS), 2015 IEEE International Geoscience and Remote Sensing Symposium (IGARSS), 2828–2831, https://doi.org/10.1109/IGARSS.2015.7326403, 2015.

Petrou, Z. I. and Tian, Y.: High-Resolution Sea Ice Motion Estimation With Optical Flow Using Satellite Spectroradiometer Data, IEEE Transactions on Geoscience and Remote Sensing, 55, 1339–1350, https://doi.org/10.1109/TGRS.2016.2622714, 2017.

Pizer, S. M., Amburn, E. P., Austin, J. D., Cromartie, R., Geselowitz, A., Greer, T., ter Haar Romeny, B., Zimmerman, J. B., and Zuiderveld, K.: Adaptive histogram equalization and its variations, Computer Vision, Graphics, and Image Processing, 39, 355–368, https://doi.org/10.1016/S0734-189X(87)80186-X, 1987.

Preller, R. H. and Posey, P. G.: A numerical model simulation of a summer reversal of the Beaufort Gyre, Geophysical Research Letters, 16, 69–72, https://doi.org/10.1029/GL016i001p00069, 1989.

Qiu, Y. and Li, X.-M.: Retrieval of sea ice drift from the central Arctic to the Fram Strait based on sequential Sentinel-1 SAR data, IEEE Trans. Geosci. Remote Sensing, 1–1, https://doi.org/10.1109/TGRS.2022.3226223, 2022.

Reimnitz, E., Dethleff, D., and Nürnberg, D.: Contrasts in Arctic shelf sea-ice regimes and some implications: Beaufort Sea versus Laptev Sea, Marine Geology, 119, 215–225, https://doi.org/10.1016/0025-3227(94)90182-1, 1994.

Rigor, I. G., Clemente-Colon, P., and Hudson, E.: The international Arctic buoy programme (IABP): A cornerstone of the Arctic observing network, in: OCEANS 2008, OCEANS 2008, 1–3, https://doi.org/10.1109/OCEANS.2008.5152136, 2008.

Schwerdtfecer, P.: The Thermal Properties of Sea Ice, Journal of Glaciology, 4, 789–807, https://doi.org/10.3189/S0022143000028379, 1963.

Serreze, M. C., Barrett, A. P., Slater, A. G., Woodgate, R. A., Aagaard, K., Lammers, R. B., Steele, M., Moritz, R., Meredith, M., and Lee, C. M.: The large-scale freshwater cycle of the Arctic, Journal of Geophysical Research: Oceans, 111, https://doi.org/10.1029/2005JC003424, 2006.

Serreze, M. C., Barrett, A. P., Stroeve, J. C., Kindig, D. N., and Holland, M. M.: The emergence of surface-based Arctic amplification, The Cryosphere, 3, 11–19, https://doi.org/10.5194/tc-3-11-2009, 2009.

Smedsrud, L. H., Halvorsen, M. H., Stroeve, J. C., Zhang, R., and Kloster, K.: Fram Strait sea ice export variability and September Arctic sea ice extent over the last 80 years, The Cryosphere, 11, 65–79, https://doi.org/10.5194/tc-11-65-2017, 2017.

https://doi.org/10.5194/egusphere-2023-1927
Preprint. Discussion started: 9 October 2023

Stern, H. L. and Moritz, R. E.: Sea ice kinematics and surface properties from RADARSAT synthetic aperture radar during the SHEBA drift, Journal of Geophysical Research: Oceans, 107, SHE 14-1-SHE 14-10, https://doi.org/10.1029/2000JC000472, 2002.

Stow, D. A., Hope, A., McGuire, D., Verbyla, D., Gamon, J., Huemmrich, F., Houston, S., Racine, C., Sturm, M., Tape, K., Hinzman, L., Yoshikawa, K., Tweedie, C., Noyle, B., Silapaswan, C., Douglas, D., Griffith, B., Jia, G., Epstein, H., Walker, D., Daeschner, S., Petersen, A., Zhou, L., and Myneni, R.: Remote sensing of vegetation and land-cover change in Arctic Tundra Ecosystems, Remote Sensing of Environment, 89, 281–308, https://doi.org/10.1016/j.rse.2003.10.018, 2004.

Sumata, H., de Steur, L., Gerland, S., Divine, D. V., and Pavlova, O.: Unprecedented decline of Arctic sea ice outflow in 2018, Nat Commun, 13, 1747, https://doi.org/10.1038/s41467-022-29470-7, 2022.

Sumata, H., de Steur, L., Divine, D. V., Granskog, M. A., and Gerland, S.: Regime shift in Arctic Ocean sea ice thickness, Nature, 615, 443–449, https://doi.org/10.1038/s41586-022-05686-x, 2023.

Thielicke, W. and Stamhuis, E. J.: PIVlab – Towards User-friendly, Affordable and Accurate Digital Particle Image Velocimetry in MATLAB, Journal of Open Research Software, 2, https://doi.org/10.5334/jors.bl, 2014.

Van Wyk de Vries, M. and Wickert, A. D.: Glacier Image Velocimetry: an open-source toolbox for easy and rapid calculation of high-resolution glacier velocity fields, The Cryosphere, 15, 2115–2132, https://doi.org/10.5194/tc-15-2115-2021, 2021.

Wagner, T. J. W., Eisenman, I., and Mason, H. C.: How Sea Ice Drift Influences Sea Ice Area and Volume, Geophysical Research Letters, 48, e2021GL093069, https://doi.org/10.1029/2021GL093069, 2021.

Wang, D.-Z., Wu, C.-H., Ip, A., Chan, C.-Y., and Wang, D.-W.: Fast Multi-template Matching Using a Particle Swarm Optimization Algorithm for PCB Inspection, in: Applications of Evolutionary Computing, Berlin, Heidelberg, 365–370, https://doi.org/10.1007/978-3-540-78761-7_39, 2008.

Wang, M., König, M., and Oppelt, N.: Partial Shape Recognition for Sea Ice Motion Retrieval in the Marginal Ice Zone from Sentinel-1 and Sentinel-2, Remote Sensing, 13, 4473, https://doi.org/10.3390/rs13214473, 2021.

Wang, X., Chen, R., Li, C., Chen, Z., Hui, F., and Cheng, X.: An Intercomparison of Satellite Derived Arctic Sea Ice Motion Products, Remote Sensing, 14, 1261, https://doi.org/10.3390/rs14051261, 2022.

Yan F., Xue W., ZhuoQi C., Gang L. I., FengMing H. U. I., and Xiao C.: Summer sea ice drift tracking and variation analysis in Fram Strait from 2011 to 2020, Chinese Journal of Geophysics, 66, 2726–2740, https://doi.org/10.6038/cjg2022Q0025, 2023.

Zuiderveld, K.: Contrast limited adaptive histogram equalization, in: Graphics gems IV, 474–485, 1994.